Isasi, I., Irusta, U., Aramendi, E., Idris, A. H., & Sörnmo, L. (2020). Restoration of the electrocardiogram during mechanical cardiopulmonary resuscitation. *Physiological Measurement*, *41*(10), 105006.

Restoration of the electrocardiogram during mechanical cardiopulmonary resuscitation

Iraia Isasi[1], Unai Irusta[1], Elisabete Aramendi[1], Ahamed H. Idris[2], Leif Sörnmo[3]

[1]Department of Communications Engineering, University of the Basque Country UPV/EHU, Bilbao, Spain
[2]University of Texas Southwestern Medical Center, Dallas, Texas, USA
[3]Department of Biomedical Engineering and Center of Integrative Electrocardiology, Lund University, Lund, Sweden

E-mail: iraia.isasi@ehu.eus

Abstract.
Objective: An artefact-free electrocardiogram (ECG) is essential during cardiac arrest to decide therapy such as defibrillation. Mechanical cardiopulmonary resuscitation (CPR) devices cause movement artefacts that alter the ECG. This study analyzes the effectiveness of mechanical CPR artefact suppression filters to restore clinically relevant ECG information.
Approach: In total, 495 10-s ECGs were used, of which 165 were in ventricular fibrillation (VF), 165 in organized rhythms (OR) and 165 contained mechanical CPR artefacts recorded during asystole. CPR artefacts and rhythms were mixed at controlled signal-to-noise ratios (SNRs), ranging from –20 dB to 10 dB. Mechanical artefacts were removed using least mean squares (LMS), recursive least squares (RLS) and Kalman filters. Performance was evaluated by comparing the clean and the restored ECGs in terms of restored SNR, correlation-based similarity measures, and clinically relevant features: QRS detection performance for OR, and dominant frequency, mean amplitude and waveform irregularity for VF. For each filter, a shock/no-shock support vector machine algorithm based on multiresolution analysis of the restored ECG was designed, and evaluated in terms of sensitivity (Se) and specificity (Sp).
Main results: The RLS filter produced the largest correlation coefficient (0.80), the largest average increase in SNR (9.5 dB), and the best QRS detection performance. The LMS filter best restored VF with errors of 10.3% in dominant frequency, 18.1% in amplitude and 11.8% in waveform irregularity. The Se/Sp of the diagnosis of the restored ECG were 95.1/94.5% using the RLS filter and 97.0/91.4% using the LMS filter.
Significance: Suitable filter configurations to restore ECG waveforms during mechanical CPR have been determined, allowing reliable clinical decisions without interrupting mechanical CPR therapy.

1. Introduction

Out-of-hospital cardiac arrest (OHCA) is a major public health problem claiming over 50 lives per 100 000 persons each year [1]. The latest guidelines from the European Resuscitation Council and the American Heart Association (AHA) identify early defibrillation and high quality cardiopulmonary resuscitation (CPR) as key therapies [2]. In particular, uninterrupted chest compressions, provided either by rescuers or through mechanical devices, are of critical importance [3]. Whereas basic life support responders rely on the defibrillator's automated analysis of the ECG for a shock/no-shock decision, advanced life support (ALS) clinicians visually evaluate the ECG to decide suitable therapeutic interventions. In both cases, chest compressions must be stopped to avoid the confounding effects of CPR artefacts on the ECG. However, such CPR interruptions produce no-flow periods that deteriorate the circulatory state of the patient, reducing the probability of successful defibrillation and subsequent survival [3].

Several adaptive filters have been designed to remove chest compression artefacts during manual CPR so that the ECG is restored [4, 5]. The first solutions used reference signals such as compression depth [6,7], thoracic impedance [6,7], compression force [8] or blood pressure [9] to model CPR artefacts. The artefacts were estimated using Wiener filters [7], recursive adaptive matching pursuit algorithms [10], Kalman filters [11], recursive least squares (RLS) [8] and Gabor filters [9], among others. The filters became considerably simplified with the introduction of a quasi-periodic CPR artefact model in which the time-varying Fourier coefficients were estimated using LMS, RLS or Kalman filters [12–14]. In this model, an estimate of the instantaneous chest compression frequency during manual CPR is required, which must be estimated from additional reference channels like depth [12], force [15] and impedance [16]. At present, mechanical CPR devices are increasingly used in resuscitation by ALS clinicians [2,17,18]. Such devices deliver chest compressions at a fixed rate and depth and, consequently, no reference channels are needed for adaptive filters based on the Fourier-series model [19,20].

The preferred approach to evaluating filter performance in terms of ECG waveform restoration is to analyze artificial mixtures of artefact-free ECGs recorded during OHCA and CPR artefacts obtained in the absence of electrical activity of the heart (asystole) [6,7]. Mixtures are formed at different signal-to-noise-ratios (SNRs), so that the clean ECG and the restored ECG (obtained by filtering) can be compared in terms of performance measures such as the restored SNR [11], or the diagnostic accuracy of an automated shock/no-shock decision algorithm [8]. In the latter case, performance is reported in terms of sensitivity (Se) and specificity (Sp), the proportion of correctly classified shockable and non-shockable rhythms, respectively [14]. Studies based on artificial mixtures, using ECGs recorded during OHCA, have only been conducted during manual CPR, however, little is known on which filter configurations offer good restoration of the ECG waveforms. Moreover, the mixture model is well-suited for evaluating ECG waveform restoration in relation to other diagnostic OHCA scenarios

such as the prediction of defibrillation success [21], the detection of pulse [22] and the prediction of re-arrest [23]. The effect of filtering on ECG restoration for those scenarios has not been yet thoroughly studied.

This study addresses the above-mentioned knowledge gaps by using a mixture model to evaluate the performance of adaptive filters during mechanical CPR in terms of ECG waveform restoration, clinically relevant ECG characteristics and shock/no-shock diagnostic accuracy. The manuscript is organized as follows: Section II describes the study dataset; Section III explains the mixture model, describes the adaptive filters and proposes novel performance measures for filter evaluation; the results, discussion and conclusions are presented in Sections IV and V.

2. Materials

The data were collected by the Dallas-Fort Worth Center for Resuscitation Research between 2012 and 2016, as part of the Resuscitation Outcomes Consortium. A cohort of 393 anonymized OHCA patient data files recorded by the MRx monitor–defibrillator (Philips Medical Systems, Andover, MA, USA) during treatment were used. CPR was administered manually or with the LUCAS-2 (Physio-Control Inc/Jolife AB, Lund, Sweden) piston-driven mechanical CPR device. The LUCAS-2 delivers chest compressions at a fixed rate of $100\,\mathrm{min}^{-1}$ with a fixed depth of 5 cm. The MRx acquires the ECG with a resolution of 1.03 µV per least significant bit, a bandwidth defined by 0 Hzand50 Hz, and a sampling frequency of 250 Hz. The ECG and the available signals to monitor chest compression activity (compression depth and impedance) were converted to Matlab (MathWorks Inc, Natick, MA, USA). Chest compressions were automatically detected using standard algorithms on the compression depth or impedance channels [15].

Signal segments of 10-s duration were extracted from the patient files to form mixtures of clean ECG and mechanical CPR artefacts during asystole. Thus, all ECGs (rhythms and CPR artefacts) come from real OHCA data recorded during treatment. The clean ECG segments were extracted in intervals with confirmed absence of chest compressions, and included 165 segments from 96 patients during shockable ventricular fibrillation (VF) and 165 segments from 165 patients in non-shockable organized rhythms (ORs). CPR artefact segments during asystole were obtained during confirmed use of LUCAS-2, indicated by a fix compression rate of $100\,\mathrm{min}^{-1}$ without variability. Asystole was confirmed during pauses in chest compressions whenever the clean ECG had a peak-to-peak amplitude below 100 µV [24]. A total of 165 CPR artefacts from 149 patients were used.

All segments (VF, OR and CPR artefacts) were band-pass filtered between 0.5 – 40 Hz to remove baseline wander and high frequency noise. A Hampel filter was used to remove spiky artefacts.

3. Methods

Figure 1 summarizes the procedure followed to evaluate the performance of the adaptive filters. First, using a mixture model, noisy ECGs are formed at controlled SNRs. Then, using different filter types and filter parameter settings, the ECGs are restored. Finally, performance is evaluated in terms of measures quantifying the similarity between the clean and the restored ECG, clinically relevant ECG waveform characteristics and accuracy of shock/no-shock decision.

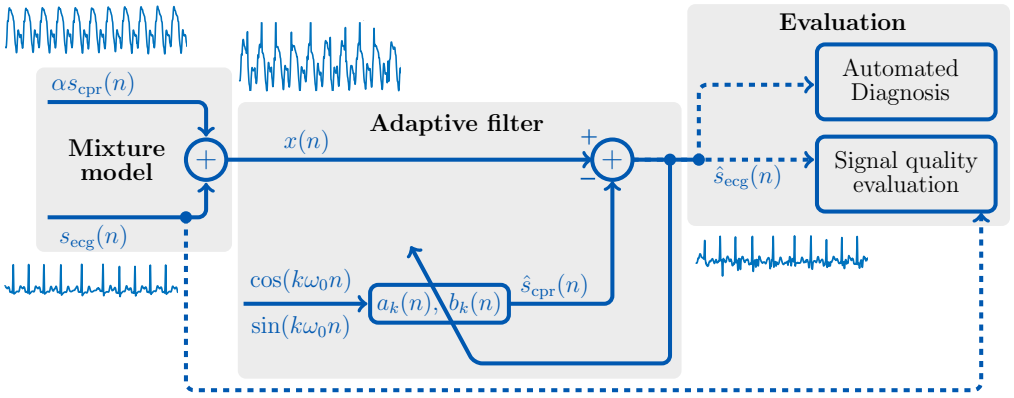

Figure 1. General architecture for CPR artefact removal and evaluation of the quality of the restored ECG, $\hat{s}_{\text{ecg}}(n)$.

3.1. Mixture model with controlled SNR

The noisy ECG signal, $x(n)$, is the mixture of a clean ECG signal, $s_{\text{ecg}}(n)$, and a signal with CPR artefacts, $s_{\text{cpr}}(n)$, recorded during asystole [6, 7]:

$$x(n) = s_{\text{ecg}}(n) + \alpha s_{\text{cpr}}(n). \tag{1}$$

The SNR of $x(n)$ is controlled by the positive-valued weight α [6]:

$$\text{SNR}_{\text{in}} = 10 \cdot \log_{10}\left(\frac{P_{\text{ecg}}}{\alpha^2 P_{\text{cpr}}}\right) \quad \text{(dB)}, \tag{2}$$

where P_{ecg} and P_{cpr} denote the power of $s_{\text{ecg}}(n)$ and $s_{\text{cpr}}(n)$, respectively, which for a segment of L samples are:

$$P_{\text{ecg}} = \frac{1}{L}\sum_{n=1}^{L}|s_{\text{ecg}}(n)|^2 \quad P_{\text{cpr}} = \frac{1}{L}\sum_{n=1}^{L}|s_{\text{cpr}}(n)|^2 \tag{3}$$

The subscript "in" indicates that the SNR applies to the filter input signal $x(n)$. In terms of signal power and SNR_{in}, α is given by

$$\alpha = \sqrt{\frac{P_{\text{ecg}}}{P_{\text{cpr}}} \cdot 10^{-\frac{\text{SNR}_{\text{in}}}{10}}}. \tag{4}$$

Seven different $\mathrm{SNR_{in}}$ are tested, ranging from very low (−20 dB) to high (10 dB) in steps of 5 dB. For each filter setting, a total of $330 \cdot 165 \cdot 7 = 3.8 \cdot 10^5$ combinations are evaluated, together forming a comprehensive selection of ECGs, CPR artefacts and $\mathrm{SNR_{in}}$. Figure 2 shows an example of $x(n)$ formed using OR and VF rhythms mixed with a CPR artefact at different $\mathrm{SNR_{in}}$.

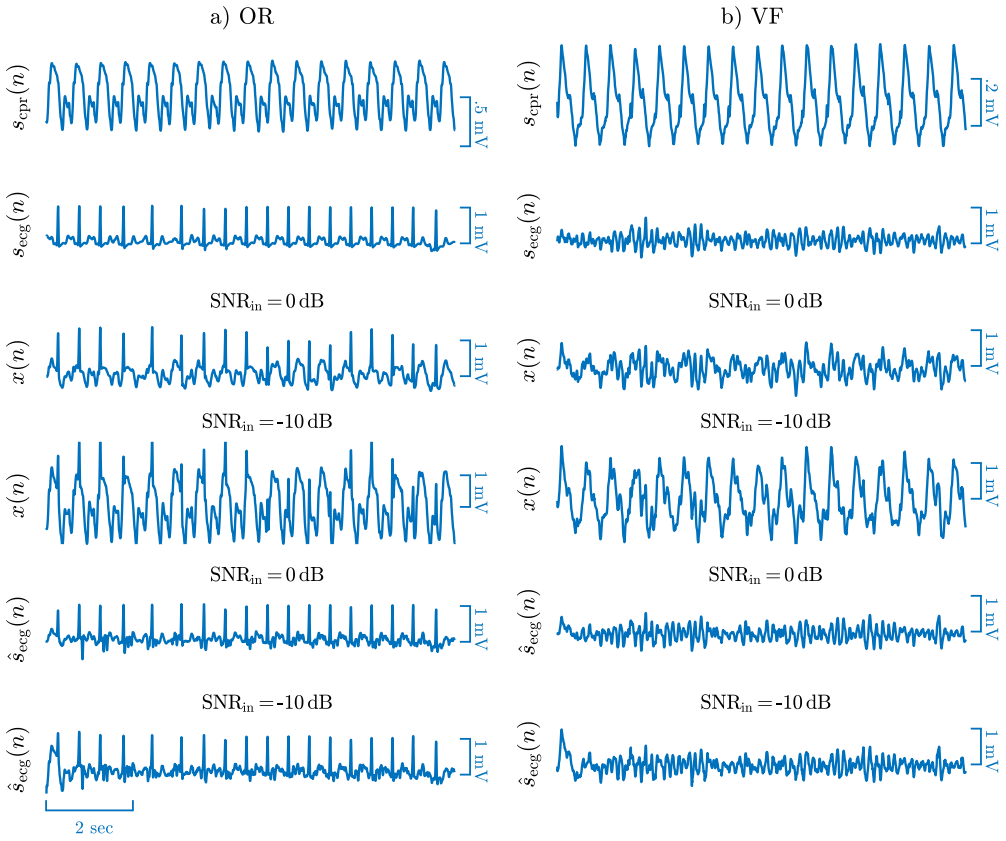

Figure 2. Examples of CPR artefact removal in ECGs with OR (a) and VF (b), using RLS filtering. CPR artefacts (panel 1), clean OR and VF signals (panel 2), mixed signals at $\mathrm{SNR_{in}}$ of 0 dB (panel 3) and −10 dB (panel 4) and restored ECGs obtained at 0 dB (panel 5) and −10 dB (panel 6).

3.2. Adaptive filters

During mechanical CPR, the chest compression frequency is constant. The LUCAS-2 device delivers compressions at $F_0 = 1.67\,\mathrm{Hz} \equiv 100\,\mathrm{min}^{-1}$, which, for a sampling period of T_s, corresponds to a discrete angular frequency of $\omega_0 = 2\pi F_0 T_\mathrm{s}$. Under this condition, the CPR artefact can be modeled as a truncated N-term Fourier series with slowly varying amplitude [25, 26]:

$$s_{\text{cpr}}(n) = \sum_{k=1}^{N} c_k(n)\cos(k\omega_0 n + \theta_k(n)) \tag{5}$$

$$= \sum_{k=1}^{N} \big(a_k(n)\cos(k\omega_0 n) + b_k(n)\sin(k\omega_0 n)\big). \tag{6}$$

The Fourier coefficients, $a_k(n)$ and $b_k(n)$, define the adaptive filter that adjust to the time-varying characteristics of the artefact [26]. The restored ECG is obtained by subtracting the model estimate $\hat{s}_{\text{cpr}}(n)$ from the observed signal $x(n)$.

$$\hat{s}_{\text{ecg}}(n) = x(n) - \hat{s}_{\text{cpr}}(n). \tag{7}$$

The LMS, RLS and Kalman filters are explored for estimating $a_k(n)$ and $b_k(n)$. All filter types employ criteria to minimize the error between $x(n)$ and $\hat{s}_{\text{cpr}}(n)$. A detailed description of the filters can be found in [25–28]. Briefly, the LMS filter updates its coefficients at each time n using increments proportional to the squared error and the step-size μ [12]. The RLS filter extends the observation window of the squared error by means of an exponential forgetting factor, λ [13]. The Kalman filter is based on a state-variable model in which the variance of the observation noise, q, controls the adjustment rate of the coefficients [14]. These three parameters control the coarseness of the respective filters. A large forgetting factor (λ), a small step size (μ) and a small noise variance (q) mean lower misadjustment and better filter stability, but reduced tracking capabilities ("fine filtering"). The reverse choice of parameter values means better tracking, but higher misadjustment and poorer stability ("coarse filtering").

In this study, three different settings of the filter parameters μ, λ and q are tested to evaluate the effect of fine, moderate and coarse filtering [14, 26], namely $\lambda = \{0.9999, 0.995, 0.99\}$, $\mu = \{15 \cdot 10^{-4}, 4 \cdot 10^{-3}, 8 \cdot 10^{-3}\}$ and $q = \{5 \cdot 10^{-6}, 1 \cdot 10^{-5}, 5 \cdot 10^{-5}\}$ [14,20,25,26]. For all cases, a model with $N = 20$ harmonics was used [26] meaning that the filters are composed of $2N$ coefficients since each harmonic is defined by a pair of coefficients (a_k, b_k). Figure 2 shows an example of $\hat{s}_{\text{ecg}}(n)$, obtained after removing CPR artefacts from $x(n)$, formed at 0 dB and at 10 dB with VF and OR as underlying rhythms.

3.3. Evaluation of filter performance

The performance is evaluated in two ways: First, by comparing $s_{\text{ecg}}(n)$ and $\hat{s}_{\text{ecg}}(n)$ using similarity measures, and by studying the effect of filtering on clinically relevant ECG waveform characteristics. Second, by building a machine learning shock advice algorithm to classify $\hat{s}_{\text{ecg}}(n)$ and thus to evaluate the accuracy of an automated diagnosis at different SNR_{in}. To avoid the influence of filter transients, performance measures are evaluated using the L samples in the interval [2.5, 9.5] s.

3.3.1. Restored signal quality measures: Three measures are computed, namely the SNR of the restored signal and two signal similarity measures. The restored SNR is defined by [6]:

$$\mathrm{SNR}_{\mathrm{res}} = 10 \cdot \log_{10}\left(\frac{P_{\mathrm{ecg}}}{P_e}\right), \tag{8}$$

where P_{ecg} and P_e are the power of $s_{\mathrm{ecg}}(n)$ and $e(n) = s_{\mathrm{ecg}}(n) - \hat{s}_{\mathrm{ecg}}(n)$, respectively.

Signal quality is quantified by Pearson's correlation coefficient (PCC) computed between $s_{\mathrm{ecg}}(n)$ and $\hat{s}_{\mathrm{ecg}}(n)$ (both signals assumed to be zero mean):

$$\mathrm{PCC} = \frac{\sum_{n=1}^{L} s_{\mathrm{ecg}}(n) \cdot \hat{s}_{\mathrm{ecg}}(n)}{\sqrt{\sum_{n=1}^{L} s_{\mathrm{ecg}}^2(n)} \cdot \sqrt{\sum_{n=1}^{L} \hat{s}_{\mathrm{ecg}}^2(n)}}, \tag{9}$$

which is a standard measure of morphological signal similarity. Values close to ± 1 indicate similarity, while values around 0 indicate dissimilarity. PCC is invariant to differences in signal amplitude, being a disadvantage in our context because filtering affects signal amplitude. For instance, VF waveform amplitude conveys important information on the state of the myocardium during cardiac arrest [21].

The adaptive signed correlation index (ASCI) reflects the amplitude differences between two signals and is defined by [29]:

$$\mathrm{ASCI} = \frac{1}{L}\sum_{n=1}^{L} s_{\mathrm{ecg}}(n) \otimes \hat{s}_{\mathrm{ecg}}(n), \tag{10}$$

where $\otimes$ denotes the signed product of two dichotomized values:

$$s_{\mathrm{ecg}}(n) \otimes \hat{s}_{\mathrm{ecg}}(n) \equiv \begin{cases} 1 & |s_{\mathrm{ecg}}(n) - \hat{s}_{\mathrm{ecg}}(n)| \leq \beta, \\ -1 & |s_{\mathrm{ecg}}(n) - \hat{s}_{\mathrm{ecg}}(n)| > \beta. \end{cases} \tag{11}$$

where the threshold β determines whether the samples at time n are similar. The threshold was set to 10% of the amplitude range of $s_{\mathrm{ecg}}(n)$, as recommended in [30]. ASCI ranges from -1 (i.e. dissimilar signals) to 1 (i.e. similar signals). In this study, ASCI is then normalized to the interval [0,1] to make it comparable to PCC.

3.3.2. Characteristic parameters of OR and VF: The most distinctive characteristic of OR is the presence of QRS complexes. Accurate detection and characterization of QRS complexes are clinically important in cardiac arrest, for example, when detecting spontaneous pulse [31]. However, QRS detection in cardiac arrest is more challenging due to frequently occurring aberrant QRS morphologies [31]. In this study, we evaluate the performance of a wavelet-based QRS detector [32] on both $s_{\mathrm{ecg}}(n)$ and $\hat{s}_{\mathrm{ecg}}(n)$. As ground truth, all QRS complexes in the 165 clean ORs are manually annotated. Finally, the occurrence times are compared to those obtained from $\hat{s}_{\mathrm{ecg}}(n)$ so that the probability of detection ($\mathrm{P_D}$) and the probability of false alarm ($\mathrm{P_F}$) can be estimated:

$$\mathrm{P_D}(\%) = 100 \cdot \frac{N_{\mathrm{TP}}}{N_{\mathrm{TP}} + N_{\mathrm{FN}}}, \tag{12}$$

$$\mathrm{P_F}(\%) = 100 \cdot \frac{N_{\mathrm{FP}}}{N_{\mathrm{TP}} + N_{\mathrm{FP}}}, \tag{13}$$

where N_{TP}, N_{FP} and N_{FN} denote the number of true positive, false positive and false negative detections, respectively.

Three characteristics of VF are studied: dominant frequency (DF) [33], amplitude [34] and waveform irregularity [21], previously used to predict defibrillation success [21, 35] and to detect VF in shock advice algorithms [13, 26, 36]. The DF is obtained by the location of the largest spectral peak higher than 1.5 Hz. The mean amplitude (MA) is obtained as the mean of $|\hat{s}_{\mathrm{ecg}}(n)|$ [21, 33]. Waveform irregularity is characterized by the sample entropy (SampEn). For the generic parameter K, the absolute relative error, ϵ, is used to evaluate filter performance:

$$\epsilon_K = 100 \times \frac{|K - \hat{K}|}{|K|} \quad \% \tag{14}$$

where K is computed from $s_{\mathrm{ecg}}(n)$ and its estimate $\hat{K}$ from $\hat{s}_{\mathrm{ecg}}(n)$, respectively.

3.4. Accuracy of automated diagnosis

Filter performance is also evaluated in terms of Se for VF and Sp for OR of a shock advice algorithm designed to classify $\hat{s}_{\mathrm{ecg}}(n)$, using a recently introduced machine learning approach for rhythm classification during mechanical CPR [26]. The algorithm is based on high-resolution feature extraction from $\hat{s}_{\mathrm{ecg}}(n)$ using the stationary wavelet transform (SWT), a wrapper-based feature selection, and a radial basis function kernel support vector machine (SVM) classifier. Details on the method for feature extraction and feature selection can be found in [26].

Data is partitioned patient-wise and stratified into training (50%), validation (20%) and test (30%) sets. The training and validation sets are used to select the most discriminative subset of 6 features, and to optimize the hyperparameters of the SVM classifier. The features are standardized to zero mean and unit variance using the data in the training set. This resulted in a training set of M instance-labeled pairs $\{(\boldsymbol{x}_1, y_1), ..., (\boldsymbol{x}_M, y_M)\} \in \mathbb{R}^6 \times \{\pm 1\}$, where $\boldsymbol{x}_i$ is the feature vector and $y_i = 1$ and $y_i = -1$ are the associated shockable and non-shockable rhythm labels, respectively. The decision function of the SVM is found by solving the following maximization problem [37]:

$$W(\alpha) = \sum_{i=1}^{M} \alpha_i - \frac{1}{2} \sum_{i,j=1}^{M} \alpha_i \alpha_j y_i y_j \exp(-\gamma \|\boldsymbol{x}_i - \boldsymbol{x}_j\|^2) \tag{15}$$

subject to the constraints:

$$0 \leq \alpha_i \leq C \quad \forall i, \quad \text{and} \quad \sum_{i=1}^{M} \alpha_i y_i = 0, \tag{16}$$

where α_i are the Lagrange multipliers which are non-zero only for M_s support vectors, C is the soft margin parameter and γ the width of the Gaussian kernel. Once the support vectors are determined, the decision function is given by:

$$f(\boldsymbol{x}) = \text{sign}\left[\sum_{i=1}^{M_s} \alpha_i y_i \exp(-\gamma \|\boldsymbol{x} - \boldsymbol{x}_i\|^2) + b\right], \tag{17}$$

where the threshold b is determined in the optimization phase and $\boldsymbol{x}$ is the feature vector under evaluation. A rhythm is classified as shockable when $f(\boldsymbol{x}) = 1$ and nonshockable when $f(\boldsymbol{x}) = -1$. The hyperparameters C and γ are determined after feature selection in the training and validation sets, using a 18×18 logarithmic grid search within $10^{-1} \leq C \leq 10^2$ and $10^{-3} \leq \gamma \leq 10^1$ to maximize the balanced accuracy (BAC), i.e. the unweighted mean of Se and Sp.

Clean ECGs and CPR artefact segments were treated as two independent databases. Each database was partitioned patient-wise and stratified into training (50%), validation (20%) and test (30%) sets. This means that $\approx 0.5 \cdot 330$ clean ECGs (131 patients) and $\approx 0.5 \cdot 165$ CPR artefact segments (74 patients) were included in the training set. The validation set consisted of $\approx 0.2 \cdot 330$ (52 patients) and $\approx 0.2 \cdot 165$ (30 patients) clean ECGs and CPR artefact segments, respectively. Finally, in the test set $\approx 0.3 \cdot 330$ clean ECGs (78 patients) and $\approx 0.3 \cdot 165$ CPR artefact segments (45 patients) were included. Thus, for each filter setting, the training, validation and test sets consist of all possible combinations of CPR artefacts and clean ECGs, mixed at the SNR_{in} levels resulting in a training set of $\approx 0.5^2 \cdot 165 \cdot 330 \cdot 7$, a validation set of $\approx 0.2^2 \cdot 165 \cdot 330 \cdot 7$ and a test set of $\approx 0.3^2 \cdot 165 \cdot 330 \cdot 7$ signals. The performance on the test set is evaluated in terms of Se, Sp and BAC.

4. Results

4.1. Signal quality

Figure 3 shows the signal quality measures as a function of SNR_{in} for different filter settings. Figure 3a shows, as expected, that $\hat{s}_{\text{ecg}}(n)$ and $s_{\text{ecg}}(n)$ become increasingly similar as SNR_{in} increases. The RLS filter leads to higher PCC and ASCI for almost all SNR_{in} when fine filters are used. However, for the Kalman and LMS filters, coarse filtering leads to higher PCC and ASCI when the CPR artefact is large. In the LMS filter, moderate filtering achieves the highest PCC and ASCI for $\text{SNR}_{\text{in}} \leq -10\,\text{dB}$, whereas coarse Kalman filtering gives the best results for $\text{SNR}_{\text{in}} \leq -10\,\text{dB}$. Figure 3b shows that coarse filtering leads to higher SNR_{res} at low SNR_{in}. However, for a low SNR_{in}, fine filtering better restores the ECG. The effect of fine and coarse filtering at a high and a low SNR_{in} is exemplified in Figure 4.

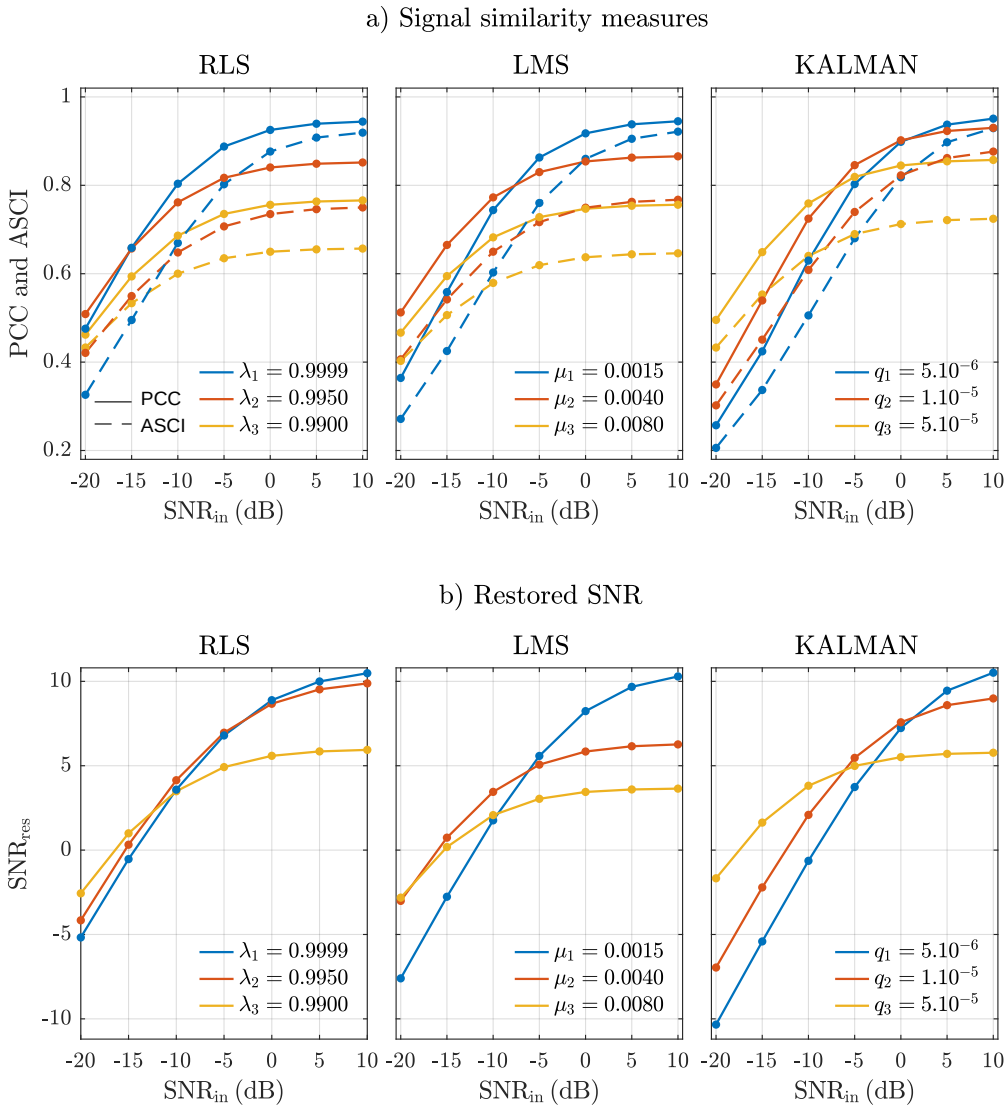

Figure 3. The mean of PCC and ASCI (a) and SNR_{res} (b) for all possible mixing combinations as a function of SNR_{in} for different filter types and settings.

4.2. Waveform characteristics

The performance of the QRS detector on clean ECGs is $P_D = 95.9\%$ and $P_F = 1.9\%$, a result which serves as an upper bound for the results obtained when artefacts are added at different SNR_{in}. Figure 5 shows the QRS detection performance obtained on $\hat{s}_{ecg}(n)$. The best performance at high SNR_{in} is obtained for the Kalman filter, but the best overall performance is obtained for the RLS filter, with P_D exceeding 90% even for an SNR_{in} around -10 dB. As SNR_{in} decreases, P_F degrades considerably for any filter type and setting. For fine RLS filtering, P_F drops from around 10% for $SNR_{in} = 5$ dB to over 30% for $SNR_{in} = -10$ dB.

The effect of filtering on VF waveform characteristics is shown in Figure 6. The absolute relative errors of DF, MA and SampEn are large at low SNR_{in}, unless coarse

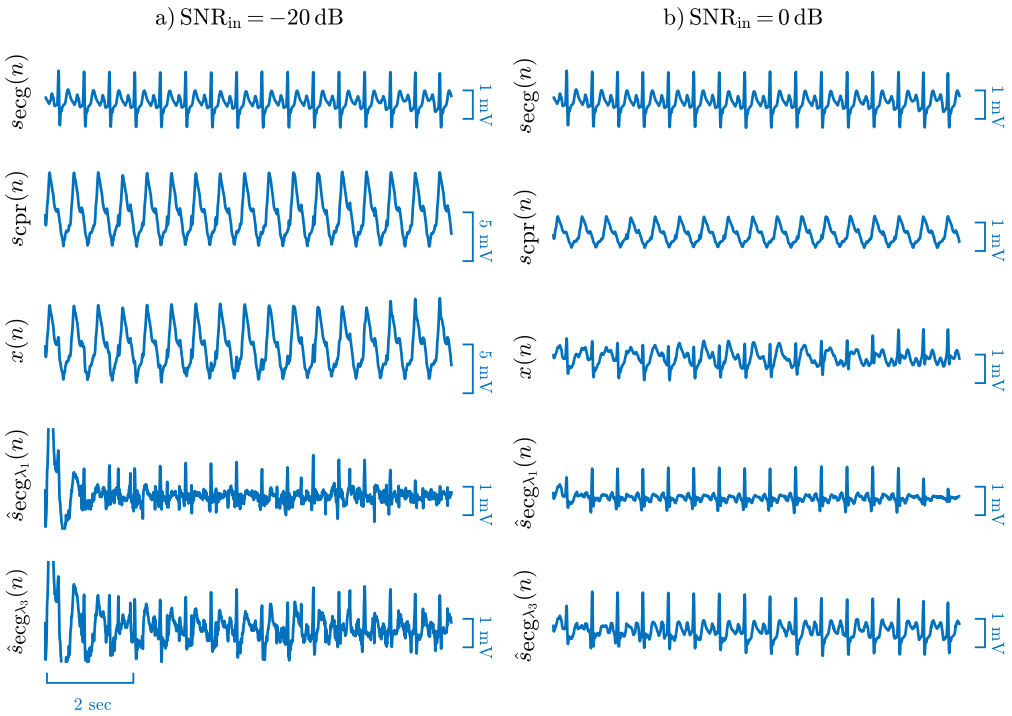

Figure 4. Two examples of RLS filtering of OR at $SNR_{in} = -20\,dB$ (a) and $0\,dB$ (b). Coarse filtering ($\lambda_3 = 0.99$) attenuates QRS amplitude more than fine filtering ($\lambda_1 = 0.9999$) which, on the other hand, produces a larger residual between QRS complexes.

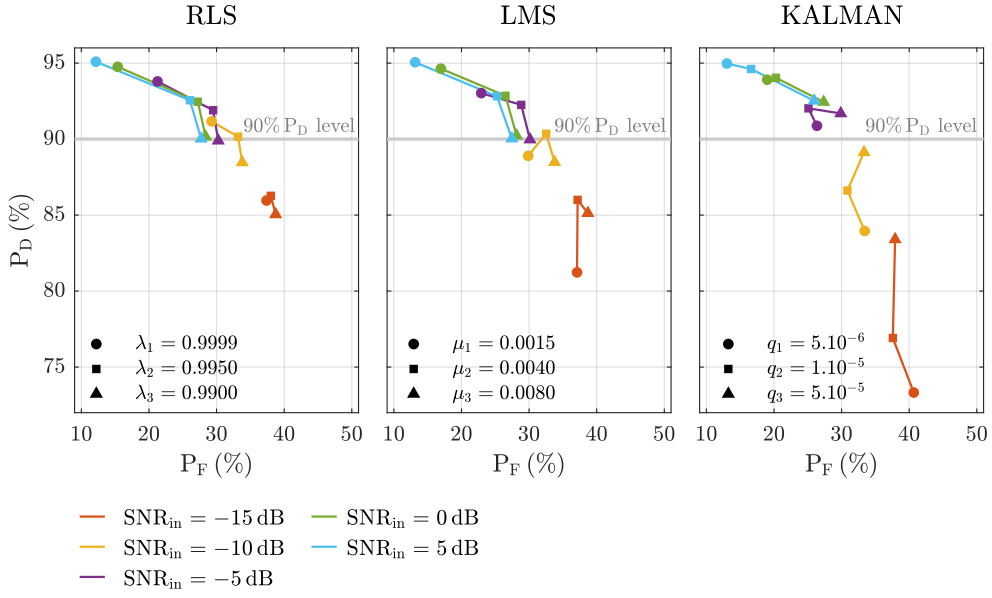

Figure 5. The mean of P_D as a function of the mean of P_F for different filter types, filter settings and SNR_{in}. Different filter settings are indicated by marker type whereas SNR_{in} by line color. The 90% P_D level is highlighted by a grey line.

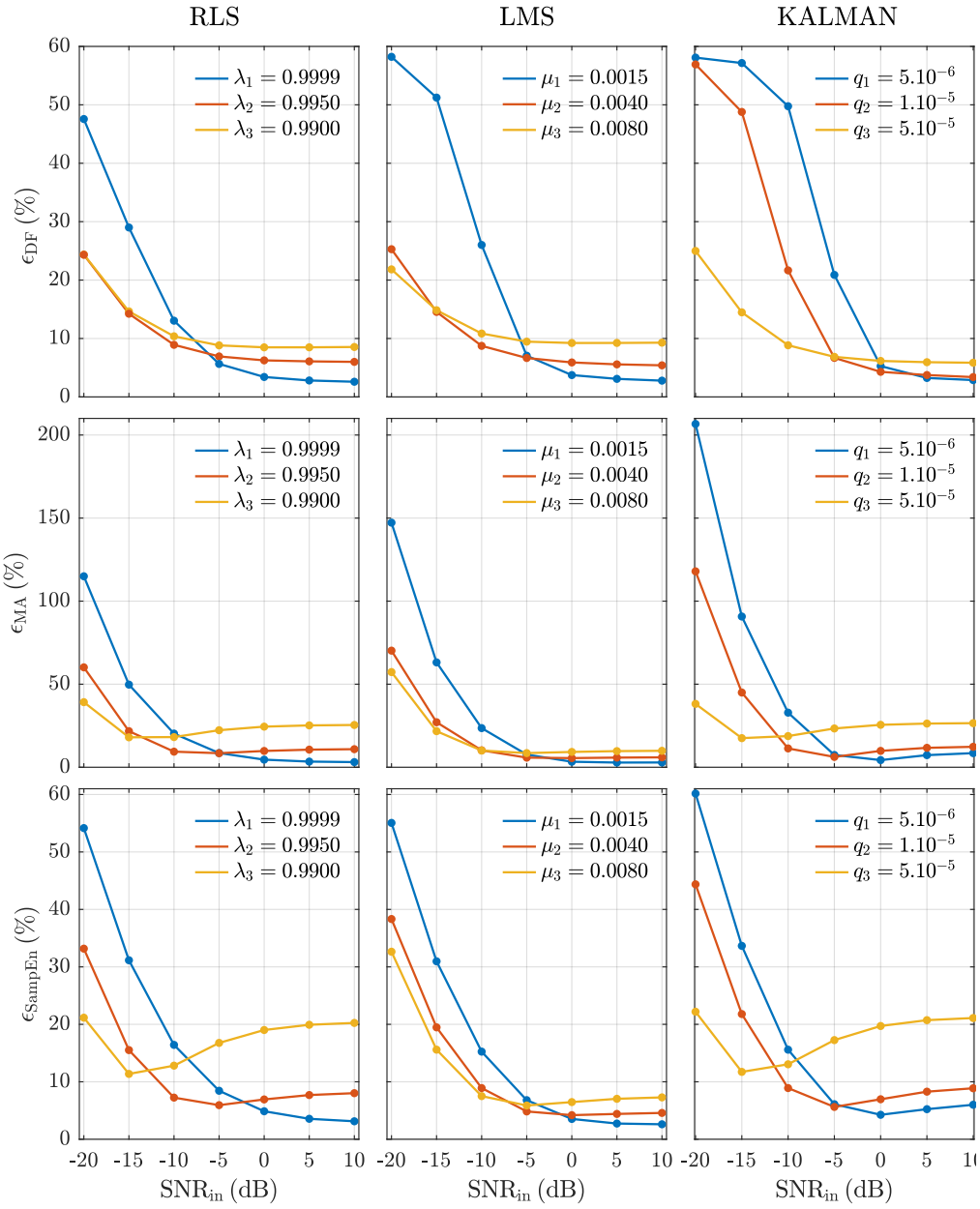

Figure 6. The mean absolute relative error of DF, MA and SampEn as a function of λ, μ, q and $\mathrm{SNR}_{\mathrm{in}}$ for different filter types and settings.

filtering is used. The error of DF is lower than 30% for $\mathrm{SNR}_{\mathrm{in}} \leq -5$ when coarse filtering is used. For large $\mathrm{SNR}_{\mathrm{in}}$, the DF of the restored VF signal is best preserved using moderate and fine filtering. The errors of MA and SampEn follow a similar pattern, with the LMS filter being the best filter overall, especially for $\mathrm{SNR}_{\mathrm{in}}$ above $-10\,\mathrm{dB}$. The RLS and Kalman filters show a degradation in the estimation of amplitude and complexity for moderate and coarse filtering as $\mathrm{SNR}_{\mathrm{in}}$ increases, possibly caused by spiky filtering residuals.

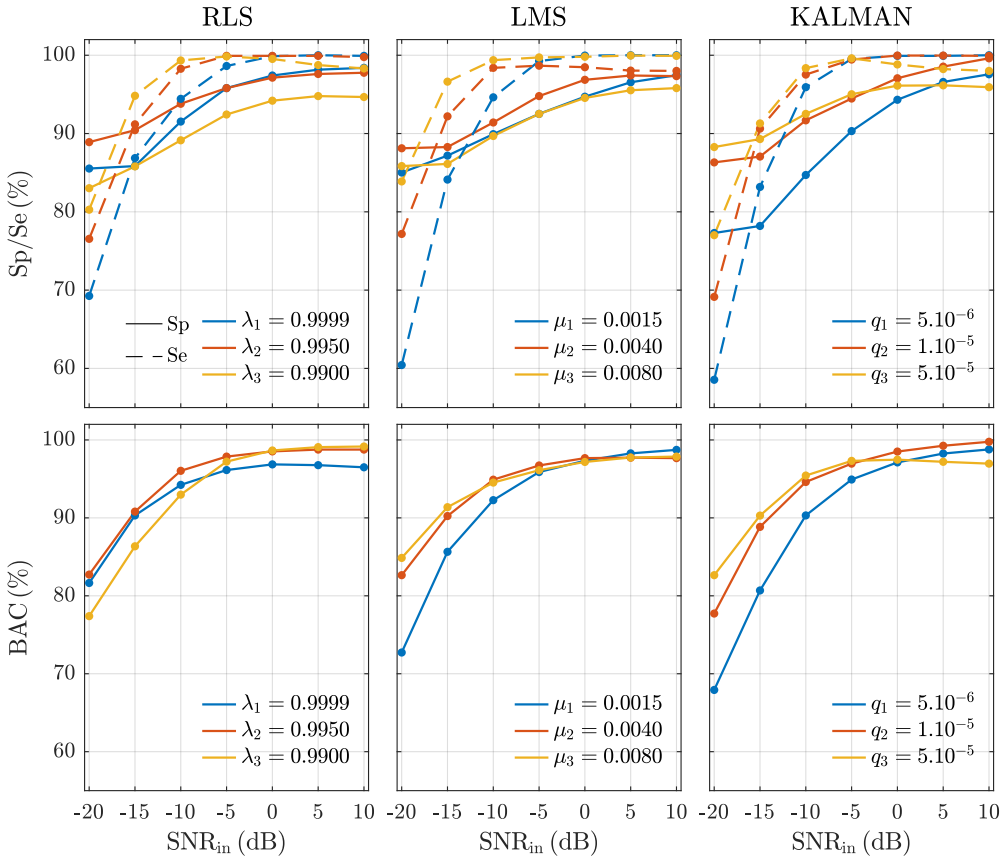

Figure 7. Performance of the shock/no-shock diagnosis for different filter types and settings.

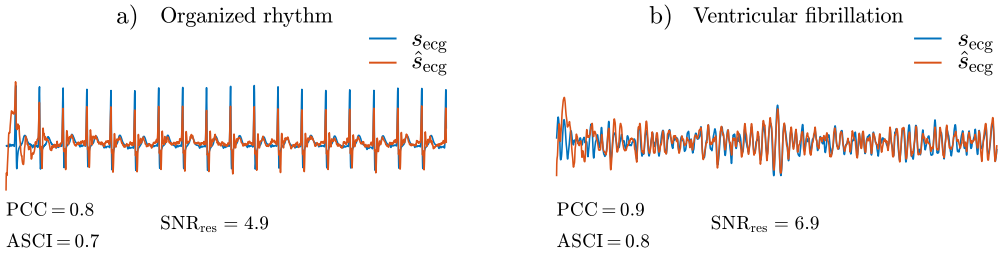

Figure 8. Effect of filtering on the amplitude of $s_{\text{ecg}}(n)$ for OR (a) and VF (b) at $\text{SNR}_{\text{in}} = -10\,\text{dB}$.

4.3. Shock/no-shock classification

The performance of the classifiers on the test set is shown in Figure 7 as a function of SNR_{in}. For most filter settings, Se and Sp are almost constant for SNR_{in} above $-5\,\text{dB}$. Moderate filtering yields better classification of OR (higher Sp), whereas coarse filtering yields better classification of VF (higher Se). The best overall performance in terms of BAC is obtained for the RLS filter, though the differences between the three filter settings are small. The Kalman filter is associated with the worst classification results, suggesting that the state-space model may not be an efficient approach for estimating

the CPR artefact model in (6). For all $\mathrm{SNR}_{\mathrm{in}}$, the BAC of the coarse LMS filter is just marginally lower (0.6-percentage points) than that of the best RLS filter.

The accuracy of the shock/no-shock decision algorithm was tested directly on the 165 CPR artefacts (with nonshockable asystole as the underlying rhythm). After filtering the artefact with the RLS filter and $\lambda = 0.995$ (best configuration), the specificity was found to be 99.4%.

Figure 9 shows four illustrative examples of misclassified segments for both shockable (VF) and nonshockable (OR) rhythms. In Figure 9a and b the artefact presents high frequency harmonics causing fast and disorganized filtering residuals in $\hat{s}_{\mathrm{ecg}}(n)$. Thus, the filtered OR rhythm resembles VF. Figure 9c and d shows spiky and high-amplitude filtering residuals resembling an OR rhythm in patients with VF, leading to a misdiagnosis in the shock/no-shock decision algorithm.

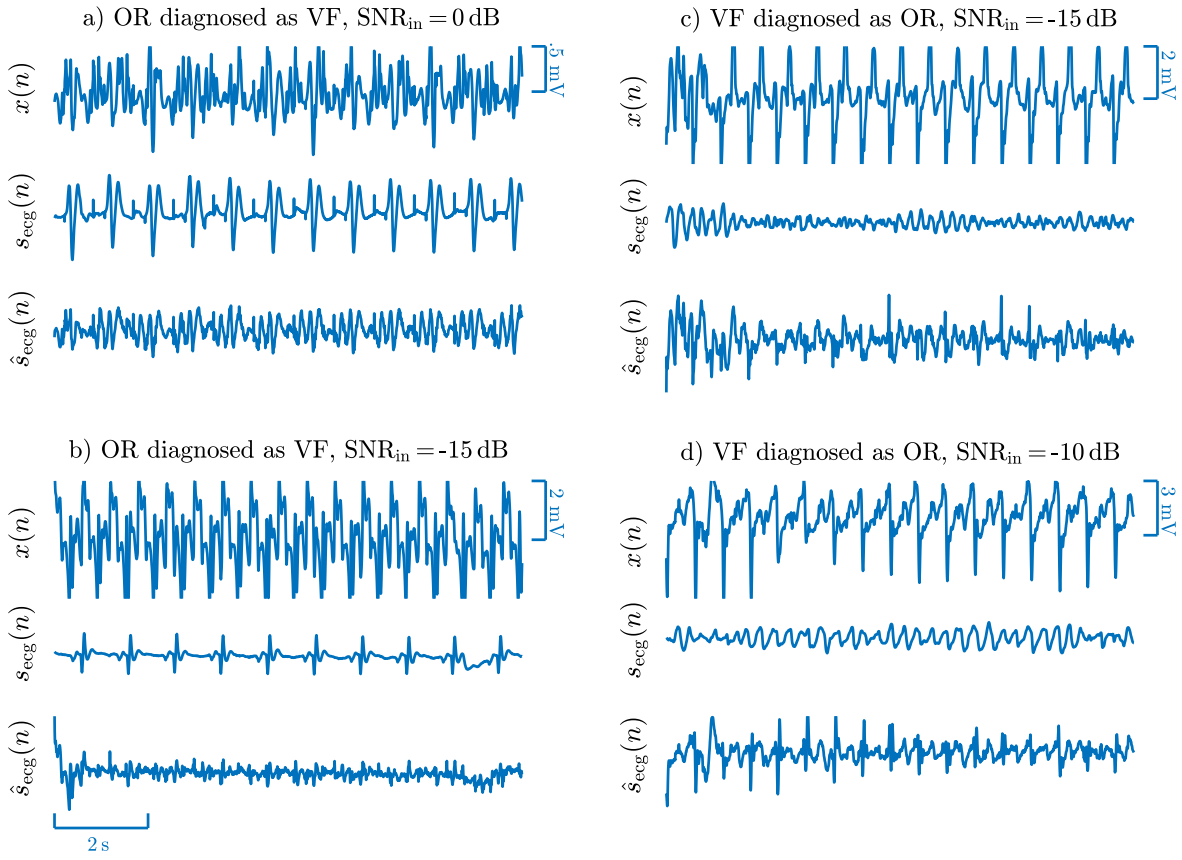

Figure 9. Examples of classification errors. Segments with OR rhythms (a,b) and segments with VF (c,d).

5. Discussion and conclusions

To the best of our knowledge, the present study provides the first thorough evaluation of ECG waveform restoration following adaptive mechanical CPR artefact cancellation

filtering. With this approach, signal quality indices and clinically relevant ECG features can be determined, providing insights into how accurately the underlying ECG rhythms can be restored with filtering. In addition to $\mathrm{SNR}_{\mathrm{res}}$, we introduce correlation-based similarity indices [30, 38] and typical OR and VF characteristics of relevance in applications such as shock outcome prediction [21, 35] and detection of pulse [22, 31]. Since ALS clinicians decide on whether to shock the patient by observing $\hat{s}_{\mathrm{ecg}}(n)$, filters that provide the highest signal quality and preserve the salient features of the rhythms are desirable. Moreover, for each filter setting, a 6-feature machine learning algorithm was adjusted to evaluate the viability of an automated shock/no-shock decision and the influence of $\mathrm{SNR}_{\mathrm{in}}$ on diagnostic accuracy during mechanical CPR.

The high values of $\mathrm{SNR}_{\mathrm{res}}$ (mean increase of 9.5 dB across all $\mathrm{SNR}_{\mathrm{in}}$) presented in Figure 3 show that adaptive filtering considerably reduces CPR artefacts, while the high correlation coefficients indicate that the ECG waveforms are quite accurately preserved in $\hat{s}_{\mathrm{ecg}}(n)$. However, the ASCI values are slightly below the PCC values suggesting an amplitude reduction in the ECG after filtering. This is illustrated in Figure 8 where $\mathrm{SNR}_{\mathrm{res}}$ is large and both PCC and ASCI are above 0.8, but ASCI is 0.1 smaller than PCC in both cases. The waveform amplitude is lower in $\hat{s}_{\mathrm{ecg}}(n)$ than in $s_{\mathrm{ecg}}(n)$.

Besides waveform alterations, this work shows for the first time that filtering causes changes to the intrinsic properties of OR and VF. The performance of the QRS detector applied to $s_{\mathrm{ecg}}(n)$ is lower when compared to those obtained on standard databases [32]. However, QRS detection in cardiac arrest patients presenting ORs is known to be challenging [31], since QRS complexes may be wide and have aberrant morphologies. As expected, the performance is lower when the QRS detector is applied to $\hat{s}_{\mathrm{ecg}}(n)$. As shown in Figure 5, true QRS complexes are accurately detected after filtering regardless of $\mathrm{SNR}_{\mathrm{in}}$. However, as $\mathrm{SNR}_{\mathrm{in}}$ decreases, the rate of false positives soars due to spiky filtering residuals confounded as actual heartbeats. This may not be a deleterious effect for shock decision algorithms since QRS presence may be enough for a no-shock decision [39], but the effect may confound other algorithms dependent on heart rate and QRS morphology such as the prediction of re-arrest [23] and the detection of spontaneous pulse [31, 40–42]. As for the restoration of VF characteristics, the best results are obtained for coarse filtering; all three types of filtering present a similar trend. At low $\mathrm{SNR}_{\mathrm{in}}$, fine filtering inefficiently removes the CPR artefact, causing the dominant frequency of the filtered VF to match the LUCAS-2 rate (1.67 Hz) in about one third of the cases when the best fine filtering is used ($\mathrm{SNR}_{\mathrm{in}} = -20$ dB and RLS with $\lambda = 0.9999$). This is a significant error considering that the mean (standard deviation) DF for clean VF in our data is 5.1 (1.5) Hz. For MA and SampEn, errors are also very large for fine filtering at low $\mathrm{SNR}_{\mathrm{in}}$, with relative errors in MA and SampEn in excess of 100% and 50%, respectively. The best overall filter to estimate SampEn is the coarse LMS filter, with an error rate below 30% for $\mathrm{SNR}_{\mathrm{in}} \geq -15$ dB and an error below 10% for $\mathrm{SNR}_{\mathrm{in}} \geq -10$ dB. These results may be of clinical importance as the dominant frequency, amplitude and entropies have been used as predictors of succesful defibrillations [21, 33–35, 43]. Our results suggest that the prediction of

defibrillation success during mechanical CPR may be possible without interrupting the chest compression therapy—a result in line with some recent findings on manual CPR [44].

While an ALS setting requires accurate restoration of $s_{\text{ecg}}(n)$, the shock/no-shock decision of $\hat{s}_{\text{ecg}}(n)$ is also crucial in automatic external defibrillators, used mainly by non-medical personnel. The decision algorithm implemented in this study has Sp below the 95% recommended by the AHA for $\text{SNR}_{\text{in}} < -5\,\text{dB}$. Moreover, Se is in compliance with the 90% recommended by the AHA for $\text{SNR}_{\text{in}} \geq -15\,\text{dB}$. For $\text{SNR}_{\text{in}} \leq -15\,\text{dB}$ Se is very low, meaning many false negatives. This is mostly because spiky and organized filtering residuals are interpreted as QRS complexes of organized rhythms in VF patients [26]. As SNR_{in} increases, a large portion of those false negatives are recovered leading to a significant increase in Se. Specificity remains quite constant for all SNR_{in}. The algorithmic procedure followed for shock/no-shock decision during mechanical CPR was recently demonstrated to have Se/Sp above 95% [26]. Our results suggest that a plausible explanation for those results is that SNR_{in}, in most cases, is high (above $-10\,\text{dB}$).

The SNR_{in} is unknown in real cardiac arrest data, so a filter cannot be adjusted to the SNR_{in}. Thus, the filter that on average shows the best performance should be preferred. Table 1 shows the mean performance across all SNR_{in} for each filter and type of filtering. The RLS filter offers the best preservation of waveform morphology (higher PCC and ASCI), as well as QRS detection performance in terms of P_{D}-to-P_{F} ratio. The VF waveform features are best preserved by the LMS filter, using either moderate or coarse filtering, although the results are almost identical to those of moderate RLS filtering. The best results on rhythm classification are obtained for moderate RLS filtering.

In monitor–defibrillators, the computational demands are important to consider because these devices use lower-end microprocessors and FPGAs which run many tasks in parallel. The LMS filter has much lower computational demands than either the RLS or Kalman filters because it only involves an error estimation at time n for the filter update equations. The RLS filter has recursions that involve matrix products [25], and so do the state-space equations. So the choice of adaptive filter should be a compromise between diagnostic accuracy, waveform preservation and computational demands on the monitor–defibrillator.

This study has certain limitations. Data obtained from a single piston driven device were used (LUCAS-2). This is the most widespread mechanical CPR device, whose impact on survival has been studied in two large randomized trials [2,17]. However, there are other piston driven devices on the market [45,46], and even alternative technologies based on load distribution bands [18]. Our results should generalize well to other piston driven devices, whereas the effect of filtering would need to be studied separately for devices based on load distribution bands for which the artefact characteristics are different [20,47]. Moreover, data were gathered using one type of monitor–defibrillator and from a single EMS agency. The characteristics of the ECG acquisition circuitry,

Table 1. Mean performance across all SNR_{in} for different filter types and settings.

	PCC	ASCI	P_D/P_F	ϵ_{DF}	ϵ_{MA}	ϵ_{SampEn}	Se	Sp	BAC
RLS									
$\lambda_1 = 0.9999$	**0.80**	**0.71**	**4.9**	14.9	24.7	17.4	92.7	93.2	93.0
$\lambda_2 = 0.9950$	0.76	0.65	2.9	10.4	18.7	12.1	95.1	**94.5**	**94.8**
$\lambda_3 = 0.9900$	0.68	0.59	2.8	12.0	29.2	17.3	95.8	90.6	93.2
LMS									
$\mu_1 = 0.0015$	0.76	0.68	4.6	21.7	35.8	16.7	91.2	91.9	91.6
$\mu_2 = 0.0040$	0.77	0.67	3.0	**10.3**	18.7	12.1	94.4	93.5	93.9
$\mu_3 = 0.0080$	0.68	0.58	2.8	12.1	**18.1**	**11.8**	**97.0**	91.4	94.2
KALMAN									
$q_1 = 5 \cdot 10^{-6}$	0.70	0.62	4.4	28.2	51.1	18.7	91.0	88.4	89.7
$q_2 = 1 \cdot 10^{-5}$	0.74	0.67	3.8	20.8	30.6	15.0	93.8	93.5	93.7
$q_3 = 5 \cdot 10^{-5}$	0.75	0.64	2.9	10.4	25.2	18.0	94.5	93.3	93.9

including sampling frequency, voltage resolution and bandwidths, differ slightly between devices, but should not alter our results substantially. Although different EMS agencies may have different protocols and quality of CPR, the use of a mechanical CPR device standardizes treatment. Finally, an additive mixture model was used to produce a noisy ECG by adding a CPR artefact to a clean ECG at different SNRs. This type of model was proposed in [7] and has since then been used in many studies [6,10,25,26]. However, the model may not accurately reflect the effect of CPR on heart dynamics. Although the additive mixture model is the best available model to evaluate the effect of filtering on ECG characteristics, a better way to evaluate shock/no-shock decision algorithms would be to use noisy ECGs recorded during OHCA. Therefore, a future study is justified to validate the shock/no-shock decision algorithm on real ECGs corrupted by CPR artefacts.

6. Bibliography

[1] C. Atwood, M. S. Eisenberg, J. Herlitz, and T. D. Rea, "Incidence of EMS-treated out-of-hospital cardiac arrest in Europe," *Resuscitation*, vol. 67, no. 1, pp. 75–80, 2005.

[2] G. D. Perkins, A. J. Handley, R. W. Koster, M. Castrén, M. A. Smyth, T. Olasveengen, K. G. Monsieurs, V. Raffay, J.-T. Gräsner, V. Wenzel *et al.*, "European resuscitation council guidelines for resuscitation 2015: Section 2. Adult basic life support and automated external defibrillation," *Resuscitation*, vol. 95, pp. 81–99, 2015.

[3] C. Vaillancourt, S. Everson-Stewart, J. Christenson, D. Andrusiek, J. Powell, G. Nichol, S. Cheskes, T. P. Aufderheide, R. Berg, I. G. Stiell *et al.*, "The impact of increased chest compression fraction on return of spontaneous circulation for out-of-hospital cardiac arrest patients not in ventricular fibrillation," *Resuscitation*, vol. 82, no. 12, pp. 1501–1507, 2011.

[4] S. Ruiz de Gauna, U. Irusta, J. Ruiz, U. Ayala, E. Aramendi, and T. Eftestøl, "Rhythm analysis during cardiopulmonary resuscitation: past, present, and future," *Biomed. Res. Int.*, vol. 2014, 2014.

[5] R. Affatato, Y. Li, and G. Ristagno, "See through ECG technology during cardiopulmonary resuscitation to analyze rhythm and predict defibrillation outcome," *Curr. Opin. Crit. Care*, vol. 22, no. 3, pp. 199–205, 2016.

[6] A. Langhelle, T. Eftestøl, H. Myklebust, M. Eriksen, B. T. Holten, and P. A. Steen, "Reducing CPR artefacts in ventricular fibrillation in vitro," *Resuscitation*, vol. 48, no. 3, pp. 279–291, 2001.

[7] S. O. Aase, T. Eftestøl, J. Husøy, K. Sunde, and P. A. Steen, "CPR artifact removal from human ECG using optimal multichannel filtering," *IEEE Trans. Biomed. Eng.*, vol. 47, no. 11, pp. 1440–1449, 2000.

[8] R. D. Berger, J. Palazzolo, and H. Halperin, "Rhythm discrimination during uninterrupted CPR using motion artifact reduction system," *Resuscitation*, vol. 75, no. 1, pp. 145–152, 2007.

[9] T. Werther, A. Klotz, G. Kracher, M. Baubin, H. G. Feichtinger, H. Gilly, and A. Amann, "CPR artifact removal in ventricular fibrillation ECG signals using Gabor multipliers," *IEEE Trans. Biomed. Eng.*, vol. 56, no. 2, pp. 320–327, 2008.

[10] J. H. Husøy, J. Eilevstjonn, T. Eftestøl, S. O. Aase, H. Myklebust, and P. A. Steen, "Removal of cardiopulmonary resuscitation artifacts from human ECG using an efficient matching pursuit-like algorithm," *IEEE Trans. Biomed. Eng.*, vol. 49, no. 11, pp. 1287–1298, 2002.

[11] K. Rheinberger, T. Steinberger, K. Unterkofler, M. Baubin, A. Klotz, and A. Amann, "Removal of CPR artifacts from the ventricular fibrillation ECG by adaptive regression on lagged reference signals," *IEEE Trans. Biomed. Eng.*, vol. 55, no. 1, pp. 130–137, 2007.

[12] U. Irusta, J. Ruiz, S. R. de Gauna, T. Eftestøl, and J. Kramer-Johansen, "A least mean-square filter for the estimation of the cardiopulmonary resuscitation artifact based on the frequency of the compressions," *IEEE Trans. Biomed. Eng.*, vol. 56, no. 4, pp. 1052–1062, 2009.

[13] I. Isasi, U. Irusta, A. B. Rad, E. Aramendi, M. Zabihi, T. Eftestøl, J. Kramer-Johansen, and L. Wik, "Automatic cardiac rhythm classification with concurrent manual chest compressions," *IEEE Access*, vol. 7, pp. 115 147–115 159, 2019.

[14] J. Ruiz, U. Irusta, S. R. de Gauna, and T. Eftestøl, "Cardiopulmonary resuscitation artefact suppression using a Kalman filter and the frequency of chest compressions as the reference signal," *Resuscitation*, vol. 81, no. 9, pp. 1087–1094, 2010.

[15] U. Ayala, T. Eftestøl, E. Alonso, U. Irusta, E. Aramendi, S. Wali, and J. Kramer-Johansen, "Automatic detection of chest compressions for the assessment of CPR-quality parameters," *Resuscitation*, vol. 85, no. 7, pp. 957–963, 2014.

[16] E. Aramendi, U. Ayala, U. Irusta, E. Alonso, T. Eftestøl, and J. Kramer-Johansen, "Suppression of the cardiopulmonary resuscitation artefacts using the instantaneous chest compression rate extracted from the thoracic impedance," *Resuscitation*, vol. 83, no. 6, pp. 692–698, 2012.

[17] S. Rubertsson, E. Lindgren, D. Smekal, O. Östlund, J. Silfverstolpe, R. A. Lichtveld, R. Boomars, B. Ahlstedt, G. Skoog, R. Kastberg, D. Halliwell, M. Box, H. Johan, and K. Rolf, "Mechanical chest compressions and simultaneous defibrillation vs conventional cardiopulmonary resuscitation in out-of-hospital cardiac arrest: the LINC randomized trial," *JAMA*, vol. 311, no. 1, pp. 53–61, 2014.

[18] L. Wik, J.-A. Olsen, D. Persse, F. Sterz, M. Lozano Jr, M. A. Brouwer, M. Westfall, C. M. Souders, R. Malzer, P. M. van Grunsven *et al.*, "Manual vs. integrated automatic load-distributing band CPR with equal survival after out of hospital cardiac arrest. the randomized CIRC trial," *Resuscitation*, vol. 85, no. 6, pp. 741–748, 2014.

[19] J. Sullivan, R. Walker, A. Esibov, and F. Chapman, "A digital filter can effectively remove mechanical chest compression artifact," *Resuscitation*, vol. 85, p. S41, 2014.

[20] E. Aramendi, U. Irusta, U. Ayala, H. Naas, J. Kramer-Johansen, and T. Eftestøl, "Filtering mechanical chest compression artefacts from out-of-hospital cardiac arrest data," *Resuscitation*,

vol. 98, pp. 41–47, 2016.

[21] B. Chicote, U. Irusta, R. Alcaraz, J. J. Rieta, E. Aramendi, I. Isasi, D. Alonso, and K. Ibarguren, "Application of entropy-based features to predict defibrillation outcome in cardiac arrest," *Entropy*, vol. 18, no. 9, p. 313, 2016.

[22] A. Elola, E. Aramendi, U. Irusta, J. Del Ser, E. Alonso, and M. Daya, "ECG-based pulse detection during cardiac arrest using random forest classifier," *Med. Biol. Eng. Comput.*, vol. 57, no. 2, pp. 453–462, 2019.

[23] A. Elola, E. Aramendi, U. Irusta, N. Amezaga, J. Urteaga, P. Owens, and A. H. Idris, "Machine learning techniques to predict cardiac re-arrest in out-of-hospital setting," *Circulation*, vol. 140, pp. A127–A127, 2019.

[24] A. B. Rad, T. Eftestøl, K. Engan, U. Irusta, J. T. Kvaløy, J. Kramer-Johansen, L. Wik, and A. K. Katsaggelos, "ECG-based classification of resuscitation cardiac rhythms for retrospective data analysis," *IEEE Trans. Biomed. Eng.*, vol. 64, no. 10, pp. 2411–2418, 2017.

[25] I. Isasi, U. Irusta, E. Aramendi, U. Ayala, E. Alonso, J. Kramer-Johansen, and T. Eftestøl, "A multistage algorithm for ECG rhythm analysis during piston-driven mechanical chest compressions," *IEEE Trans. Biomed. Eng.*, vol. 66, no. 1, pp. 263–272, 2018.

[26] I. Isasi, U. Irusta, A. Elola, E. Aramendi, U. Ayala, E. Alonso, J. Kramer-Johansen, and T. Eftestøl, "A machine learning shock decision algorithm for use during piston-driven chest compressions," *IEEE Trans. Biomed. Eng.*, vol. 66, no. 6, pp. 1752–1760, 2018.

[27] S. R. de Gauna, J. Ruiz, U. Irusta, E. Aramendi, T. Eftestøl, and J. Kramer-Johansen, "A method to remove CPR artefacts from human ECG using only the recorded ECG," *Resuscitation*, vol. 76, no. 2, pp. 271–278, 2008.

[28] S. Haykin, *Kalman Filtering and Neural Networks*. John Wiley & Sons, 2004, vol. 47.

[29] J. Lian, G. Garner, D. Muessig, and V. Lang, "A simple method to quantify the morphological similarity between signals," *Signal Process.*, vol. 90, no. 2, pp. 684–688, 2010.

[30] R. Alcaraz, F. Hornero, A. Martínez, and J. J. Rieta, "Short-time regularity assessment of fibrillatory waves from the surface ECG in atrial fibrillation," *Physiol. Meas.*, vol. 33, no. 6, p. 969, 2012.

[31] A. Elola, E. Aramendi, U. Irusta, E. Alonso, Y. Lu, M. P. Chang, P. Owens, and A. H. Idris, "Capnography: A support tool for the detection of return of spontaneous circulation in out-of-hospital cardiac arrest," *Resuscitation*, vol. 142, pp. 153–161, 2019.

[32] J. P. Martínez, R. Almeida, S. Olmos, A. P. Rocha, and P. Laguna, "A wavelet-based ECG delineator: evaluation on standard databases," *IEEE Trans. Biomed. Eng.*, vol. 51, no. 4, pp. 570–581, 2004.

[33] C. G. Brown and R. Dzwonczyk, "Signal analysis of the human electrocardiogram during ventricular fibrillation: frequency and amplitude parameters as predictors of successful countershock," *Ann. Emerg. Med.*, vol. 27, no. 2, pp. 184–188, 1996.

[34] W. D. Weaver, L. A. Cobb, D. Dennis, R. Ray, A. P. Hallstrom, and M. K. Copass, "Amplitude of ventricular fibrillation waveform and outcome after cardiac arrest," *Ann. Intern. Med.*, vol. 102, no. 1, pp. 53–55, 1985.

[35] B. Chicote, U. Irusta, E. Aramendi, R. Alcaraz, J. J. Rieta, I. Isasi, D. Alonso, M. Baqueriza, and K. Ibarguren, "Fuzzy and sample entropies as predictors of patient survival using short ventricular fibrillation recordings during out of hospital cardiac arrest," *Entropy*, vol. 20, no. 8, p. 591, 2018.

[36] C. Figuera, U. Irusta, E. Morgado, E. Aramendi, U. Ayala, L. Wik, J. Kramer-Johansen, T. Eftestøl, and F. Alonso-Atienza, "Machine learning techniques for the detection of shockable rhythms in automated external defibrillators," *PloS ONE*, vol. 11, no. 7, p. e0159654, 2016.

[37] B. Scholkopf, K.-K. Sung, C. J. Burges, F. Girosi, P. Niyogi, T. Poggio, and V. Vapnik, "Comparing support vector machines with Gaussian kernels to radial basis function classifiers," *IEEE Trans. Biomed. Eng.*, vol. 45, no. 11, pp. 2758–2765, 1997.

[38] M. García, M. Martínez-Iniesta, J. Ródenas, J. J. Rieta, and R. Alcaraz, "A novel wavelet-based

filtering strategy to remove powerline interference from electrocardiograms with atrial fibrillation," *Physiol. Meas.*, vol. 39, no. 11, p. 115006, 2018.

[39] U. Irusta, J. Ruiz, E. Aramendi, S. R. de Gauna, U. Ayala, and E. Alonso, "A high-temporal resolution algorithm to discriminate shockable from nonshockable rhythms in adults and children," *Resuscitation*, vol. 83, no. 9, pp. 1090–1097, 2012.

[40] E. Alonso, E. Aramendi, M. Daya, U. Irusta, B. Chicote, J. K. Russell, and L. G. Tereshchenko, "Circulation detection using the electrocardiogram and the thoracic impedance acquired by defibrillation pads," *Resuscitation*, vol. 99, pp. 56–62, 2016.

[41] M. Risdal, S. O. Aase, J. Kramer-Johansen, and T. Eftesøl, "Automatic identification of return of spontaneous circulation during cardiopulmonary resuscitation," *IEEE Trans. Biomed. Eng.*, vol. 55, no. 1, pp. 60–68, 2007.

[42] J. Ruiz, E. Alonso, E. Aramendi, J. Kramer-Johansen, T. Eftestøl, U. Ayala, and D. González-Otero, "Reliable extraction of the circulation component in the thoracic impedance measured by defibrillation pads," *Resuscitation*, vol. 84, no. 10, pp. 1345–1352, 2013.

[43] L. D. Sherman, "The frequency ratio: an improved method to estimate ventricular fibrillation duration based on Fourier analysis of the waveform," *Resuscitation*, vol. 69, no. 3, pp. 479–486, 2006.

[44] J. Coult, J. Blackwood, L. Sherman, T. D. Rea, P. J. Kudenchuk, and H. Kwok, "Ventricular fibrillation waveform analysis during chest compressions to predict survival from cardiac arrest," *Circulation*, vol. 12, no. 1, p. e006924, 2019.

[45] L. Zhang and H. Zhang, "Clinical application of Thumper in emergency cardiopulmonary resuscitation," *Baotou Medical College*, vol. 6, 2008.

[46] W. Wieczorek and H. Kaminska, "Impact of a corpuls CPR mechanical chest compression device on chest compression quality during extended pediatric manikin resuscitation: a randomized crossover pilot study," *Disaster Emerg. Med. J.*, vol. 2, no. 2, pp. 58–63, 2017.

[47] I. Isasi, U. Irusta, E. Aramendi, J. Age, and L. Wik, "Characterization of the ECG compression artefact caused by the Autopulse device," *Resuscitation*, vol. 118, p. e38, 2017.